JSR Publications

Available Online

J. Sci. Res. **16** (2), 551-560 (2024)

JOURNAL OF SCIENTIFIC RESEARCH

www.banglajol.info/index.php/JSR

Strong Red, Blue, and Yellow Emissions from Eu^{3+} and Dy^{3+}-Doped CaF_2 Nanocrystals

S. Sarkar*

Department of Chemistry, Ananda Mohan College, Kolkata, 700009, West Bengal, India

Received 9 October 2023, accepted in final revised form 14 February 2024

Abstract

This paper represents a simplistic hydrothermal method for the synthesis of lanthanide (Ln^{3+})-doped (Ln= Eu, Dy) alkaline earth metal fluoride, i.e., CaF_2 nanocrystals coated with poly(acrylic acid) (PAA). The structural and optical characterization of as-prepared nanocrystals is performed using scanning electron microscopy (SEM), powder X-ray diffraction (PXRD), Fourier transform infrared spectrum (FTIR), thermogravimetric analysis (TGA), photoluminescence spectroscopy (PL), and PL lifetime measurements. It is observed that CaF_2 exhibits strong red emission when doped with Eu^{3+} (5 mol%) ions, whereas it shows strong blue and yellow emission when doped with Dy^{3+} (2 mol%) ions. PAA coating helps to enhance the stability as well as water dispersibility of the nanocrystals. Moreover, this method can be extended to make other lanthanide-doped alkaline earth metal fluoride nanocrystals. The high photoluminescence efficiency and water solubility of the nanocrystals make the material to be used in many fields of optical devices as well as biological applications.

Keywords: Nanocrystals; Fluoride; Photoluminescence; Lanthanide; Hydrothermal.

doi: https://dx.doi.org/10.3329/jsr.v16i2.69261 J. Sci. Res. **16** (2), 551-560 (2024)

1. Introduction

Fluorescent nanomaterials have attracted much attention due to their potential applications in displays, lasers, optoelectronic devices, bioimaging, sensing, drug delivery, *etc.* [1-6]. Among various luminescent nanomaterials, lanthanide (Ln^{3+})-doped luminescent nanoparticles are immensely studied due to the interesting optical properties of lanthanide ions which arise from their unique intra 4*f*-4*f* transitions [7]. These intra 4*f*-4*f* transitions are less influenced by the ligand field due to the shielding of the 4*f* orbitals by the valance 5*s* and 5*p* orbitals, leading to sharp and narrow spectral bands [8]. However, the luminescence efficiency is comparatively better in low phonon matrices such as fluorides, a superior host for lanthanides compared to that of oxide or phosphate hosts [9-11]. This is well supported by the large number of reports that exist on fluoride nanocrystals [12-15].

There are many studies on LaF_3, YF_3, and $NaYF_4$, which are widely known in the field of luminescent nanomaterials, while reports on alkaline earth metal fluorides are

* *Corresponding author*: sarkar.shyam@gmail.com

relatively less. Alkaline earth metal fluoride nanocrystals have gained interest both for structural and optical reasons. For example, Er^{3+}/Yb^{3+}-doped CaF_2 exhibits better luminescence efficiency compared to similar dopants in $NaYF_4$ [16]. Chen *et al.* have shown that the size and shape of the SrF_2 can be modified through lanthanide doping [17]. Lin and co-workers were able to make MF_2 nanocrystals of different morphologies, like cubes, sheets, *etc*., via the solvothermal method using oleic acid as a surfactant [18]. In another study, CaF_2 nanoparticles with different hierarchical structures were prepared *via* a combined microwave and hydrothermal-assisted route using ionic liquid [19]. Very recently, a study on photoluminescence and stability of Tb^{3+}-doped CaF_2 nanoparticles without a capping agent, prepared by microwave method, is reported, and the nanoparticles are not soluble in water [20]. Hence, most of the reports above are associated with uncapped CaF_2 nanoparticles and organic solvent-dispersible CaF_2 nanocrystals. Now, to envision and broaden the application of lanthanide-doped CaF_2 nanocrystals, it is important to make them water-dispersible.

In this research article, we report the synthesis of water-dispersible Ln^{3+}-doped CaF_2 (Ln = Eu and Dy) using a simple hydrothermal method (see experimental section for details). The surface of the nanocrystals is functionalized with polyacrylic acid (PAA) molecules, which helps to make the nanocrystals' water dispersible. The reason for choosing PAA is due to the presence of a large number of carboxylic groups that can be used to bind to the nanocrystals and assist in water dispersibility. The synthesis, structural, and optical properties of lanthanide-doped nanocrystals are studied in detail. It has been found that CaF_2 exhibits very strong red emission when doped with Eu^{3+} ions, whereas it shows strong blue and yellow emission when doped with Dy^{3+} ions.

2. Materials and Methods

2.1. *Materials*

The chemicals used in this work, such as calcium nitrate [$Ca(NO_3)_2{\cdot}4H_2O$; 99 %] (Merck, India), europium nitrate [$Eu(NO_3)_3{\cdot}5H_2O$; 99.99 %] (Merck, Germany), dysprosium nitrate [$Dy(NO_3)_3$; 99.99 %] (Merck, Germany), poly(acrylic acid) [PAA, M_w=1800] (Merck India), ethylene glycol (EG, ≥99.9 %) (Merck India), sodium fluoride (NaF, ≥99 %) (Merck India) and absolute ethanol (EtOH, ≥99.5 %) (Merck, Germany) were used without further purification.

2.2. *Synthesis of nanocrystals*

Ln^{3+}-doped (Ln= Eu^{3+}, Dy^{3+}) CaF_2 nanocrystals were prepared using alkaline earth metal nitrate salts and sodium fluoride as precursors in a mixture of ethylene glycol and ethanol with PAA as the surface capping agent using our previously published work with a slight modification [21]. First, aqueous solutions of $Ca(NO_3)_2$ [0.95 mmol, 224.34 mg], and $Eu(NO_3)_3$ (0.05 mmol, 21.4 mg) were taken in a 100 mL beaker. Then this clear solution was added to a mixture of ethanol (10 mL) and ethylene glycol (10 mL), and the whole

mixture was stirred under magnetic stirring. Then sodium fluoride solution (2 mmol, 84 mg) was added to it and again stirred continuously for ~25 min. By this time, the mixture had become a white colloidal solution, PAA (0.1 g) was added to it, and the stirring was maintained for another 25 min. Subsequently, the milky colloidal mixture was transferred into a 100 mL Teflon-lined pot of an autoclave reactor. The autoclave reactor is tightly sealed and heated at 200 °C for 24 h. Then, the autoclave system was allowed to cool to room temperature. Finally, the as-synthesized nanocrystals were collected by centrifugation at 6000 rpm for 10 min. Then, the solid mass precipitated in the centrifuge tube was washed three times with ethanol and, at last, with deionized water to remove unwanted impurities (if any). The formed solid nanocrystals were dried in a vacuum desiccator for 2-3 h. Both the solid nanocrystals and 1 wt (%) aqueous solution were preserved for characterization. The whole synthetic process is summarized in the form of a schematic presentation, as shown in Scheme 1.

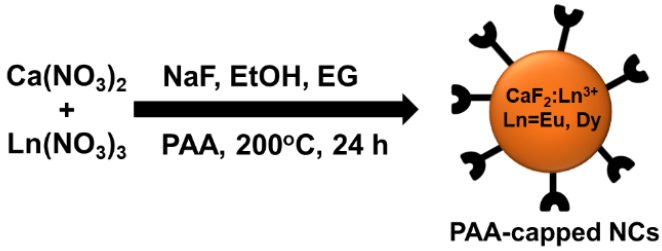

Scheme 1. Schematic presentation of the synthesis of PAA-capped Ln^{3+}-doped CaF_2 (Ln=Eu, Dy) nanocrystals.

2.3. *Analysis method*

Rigaku-Smart Lab diffractometer was used to perform Powder X-ray diffraction (PXRD) measurements for identification of phase, purity, and crystal structure. The instrument was operated at 200 kV and 45 mA at a scanning rate of 1° min^{-1} in the 2θ range from 15° to 90° with a CuK_α X-ray source. The samples were entirely fine powdered and spread well on a quartz slide. The JEOL (Model no. JSM 6390 LV) instrument was used to capture field emission scanning electron microscopy (FESEM) images for morphological information. For FESEM, all samples were coated with a thin film of platinum to avoid a charging effect before loading them into the sample chamber of the instrument. Perkin Elmer (Model No. RX_1) spectrophotometer was used to collect all the FTIR spectra in which the KBr-disk technique was applied, and the range of spectra collection was from 400 to 4000 cm^{-1}. For recording the FTIR spectra, KBr pellets were made by mixing ~200 mg of KBr and ~10 mg of the powder sample. TGA was performed at a heating rate of 10° min^{-1} using a Mettler Toledo (Model No. 851) instrument under the N_2 atmosphere. All photoluminescence (PL) spectra measurements were performed using Fluoromax-3 (Horiba Jobin Yvon), in which a steady-state 450 W Xe lamp was used to record emission spectra. The PL measurement was carried out from the aqueous solution of the

nanocrystals by exciting them at 394 nm and 350 nm, respectively, for Eu^{3+} and Dy^{3+}-doped CaF_2 nanocrystals. The photoluminescence lifetime measurements were carried out using a water solution of the nanocrystals with the Fluoromax-4 (Horiba Jobin Yvon) instrument, and the power of the pulsed Xe source was 150 W. All the measurements were performed at room temperature. All the instruments used for characterization belong to the Indian Institute of Science Education and Research (IISER), Kolkata.

3. Results and Discussion

3.1. *Phase and crystal structure analyses*

The purity, type of phase, and unit cell crystal structure of the PAA-coated Ln^{3+}-doped CaF_2 nanocrystals were performed using powder X-ray diffraction (PXRD) measurements. Fig. 1 shows the XRD patterns of the as-prepared PAA-coated bare CaF_2 nanocrystals, PAA-coated Eu^{3+} (5 mol%)-doped CaF_2 nanocrystals, and PAA-coated Dy^{3+} (2 mol%)-doped CaF_2 nanocrystals. All the diffraction peaks of these nanocrystals are well indexed with the standard diffraction lines of cubic CaF_2 crystals (ICSD PDF card No. 00-004-0864). The absence of any other impurity peaks in the XRD pattern implies that the nanocrystals are formed in a pure cubic phase. The average crystallite sizes of these nanocrystals were calculated using Debye-Scherrer's equation, $D = (0.9\ \lambda/\beta\text{Cos}\theta)$, where D is the crystallite size, λ denotes (1.5418 Å) the wavelength of the incident X-ray beams, and β is the corrected FWHM (full width at half maximum) in radians. Angle θ is the diffraction angle for the (hkl) plane. Using Debye-Scherrer's equation, the calculated average crystallite size of PAA-coated bare CaF_2 nanocrystals is found to be 23.8 nm, considering the most intense peak (111). Similarly, the crystallite size has been calculated for both PAA-coated Eu^{3+} (5 mol%)-doped and Dy^{3+}(2 mol%)-doped CaF_2 nanocrystals. The calculated crystallite size is 22.2 and 20.6 nm, respectively, for PAA-coated Eu^{3+} (5 mol%)-doped and Dy^{3+} (2 mol%)-doped CaF_2 nanocrystals. The decrease in the crystallite size indicates the successful doping of lanthanide ions (Eu^{3+} and Dy^{3+}) into the CaF_2 nanocrystals matrix.

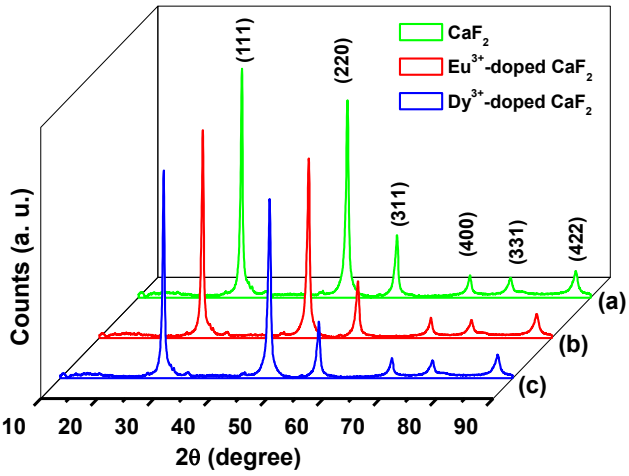

Fig. 1. PXRD patterns of PAA-coated (a) only CaF_2 nanocrystals, (b) Eu^{3+} (5 mol%)-doped CaF_2 nanocrystals, and (c) Dy^{3+}(2 mol%)-doped CaF_2 nanocrystals.

3.2. *Morphology analysis*

The morphology of as-prepared CaF_2 nanocrystals was characterized by FESEM measurements. FESEM images of PAA-coated bare CaF_2, Eu^{3+} (5 mol%)-doped CaF_2 nanocrystals, and Dy^{3+} (2 mol%)-doped CaF_2 nanocrystals are shown in Figs. 2A, 2B and 2C, respectively. It is clear from the image that nanocrystals possess spherical morphology with an average size of ~25 nm for pure CaF_2 nanocrystals. Whereas, in case of Eu^{3+} (5 mol%)-doped CaF_2 nanocrystals, and Dy^{3+} (2 mol%)-doped CaF_2 nanocrystals the size decreases to ~23 nm and ~21 nm, respectively. This decrease in the size of CaF_2 nanocrystals supports the results obtained from Debye-Scherer's calculations. This further expresses the successful doping of lanthanide ions into the CaF_2 matrix.

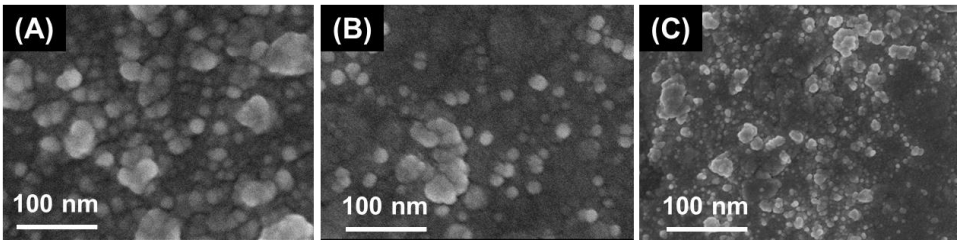

Fig. 2. FESEM images of PAA-coated (A) only CaF_2 nanocrystals, (B) Eu^{3+} (5 mol%)-doped CaF_2 nanocrystals, and (C) Dy^{3+} (2 mol%)-doped CaF_2 nanocrystals.

3.3. *Surface functionalization*

The attachment of the organic functional groups present in PAA molecules around the surface of the nanocrystals was confirmed by the FTIR spectroscopy analysis. Fig. 3 displays the FTIR spectra of the pure PAA molecules (black line), PAA-coated Eu^{3+}-doped CaF_2 nanocrystals (red line) and Dy^{3+}-doped CaF_2 nanocrystals (blue line). Pure PAA molecules showed four characteristic absorption bands in the FTIR spectrum, as shown in Fig. 3(a). The peak at 2952 cm^{-1} is assigned to the methylene (-CH_2-) stretching vibrations of the long alkyl chain of free PAA molecules. The band located at 1727 cm^{-1} is assigned to the -C=O stretching vibration of the –COOH group, and two weaker bands at 1455 cm^{-1} and 1415 cm^{-1} are associated with the stretching and bending vibrations of –CH_2– and CH–CO groups, respectively [22]. As shown in Figs. 3(b) and (c), all four characteristic PAA absorption bands are observed in both the nanocrystals, along with a new band around 1556 cm^{-1}. The C=O stretching observed at 1727 cm^{-1} for the free PAA molecules is shifted to 1556 cm^{-1} in both the nanocrystals, authenticating the binding of the carbonyl of the COOH groups attached to the nanocrystals surface. From the FTIR result, it is clear that a large number of the carboxyl groups in the PAA chains strongly coordinated to the nanocrystal surface, making them water dispersible.

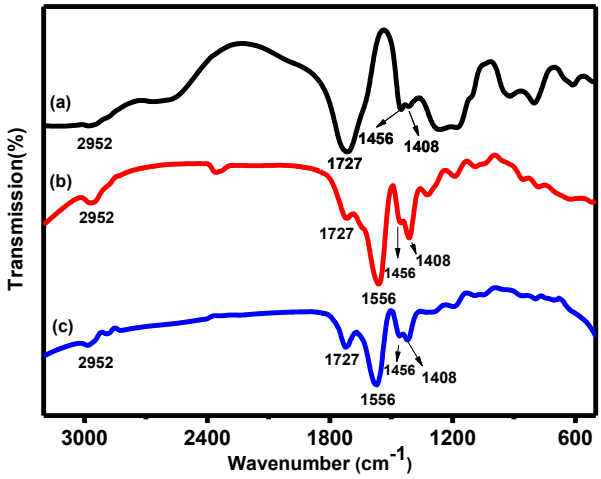

Fig. 3. FTIR spectra of (a) pure PAA molecules, (b) PAA-capped Eu^{3+} (5 mol%)-doped CaF_2 nanocrystals, and (c) PAA-capped Dy^{3+} (2 mol%)-doped CaF_2 nanocrystals.

The binding of PAA molecules over the surface of CaF_2 nanocrystals is further supported by the TGA analysis. The TGA curves for pure free PAA molecules, Eu^{3+} (5 mol%)-doped PAA capped CaF_2 nanocrystals, and Dy^{3+} (2 mol%)-doped PAA capped CaF_2 nanocrystals are shown in Fig. 4. For the pure free PAA molecules the decomposition started just above 200°C, almost ~80 % decomposition occurs over a range

of 200-500 °C temperature. Whereas for the PAA-coated Eu^{3+} (5 mol%)-doped and Dy^{3+} (2 mol%)-doped CaF_2 nanocrystals, the decomposition (~10 %) started at a comparatively much higher temperature, i.e., in the range of 400-500 ºC. It means that when the PAA molecule is free, it decomposes in a comparatively lower temperature range, but when it is attached to a nanoparticle surface, it breaks down at a high-temperature range. Thus, the TGA result further confirms that PAA molecules are strongly attached to the surface of both Eu^{3+} (5 mol%)-doped and Dy^{3+} (2 mol%)-doped CaF_2 nanocrystals.

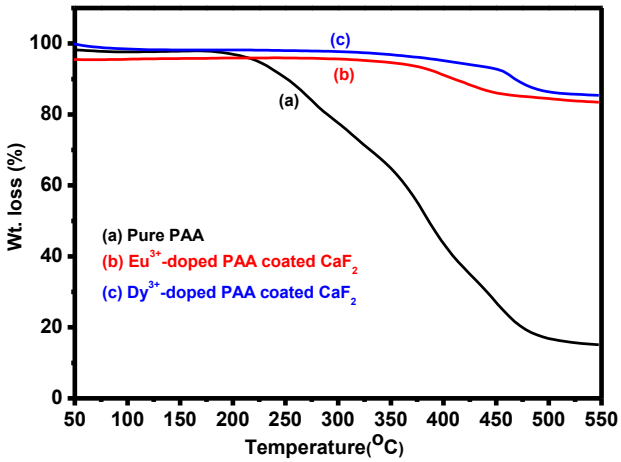

Fig. 4. TGA curves of (a) pure PAA molecules, (b) PAA-capped Eu^{3+} (5 mol%)-doped CaF_2 nanocrystals, and (c) PAA-capped Dy^{3+} (2 mol%)-doped CaF_2 nanocrystals.

3.4. *Optical properties*

Luminescence properties of Ln^{3+}-doped CaF_2 nanocrystals are characterized by photoluminescence (PL) spectroscopy. Fig. 5(A) represents the photoluminescence emission spectra of Eu^{3+} (5 mol%)-doped CaF_2 nanocrystals in water. The intense emission bands at 591, 614, 651, and 702 nm are, respectively, due to the transitions from $^5D_0$ to $^7F_1$, $^7F_2$, $^7F_3$, and $^7F_4$ levels. Emission spectra were collected by exciting the water dispersion of Eu^{3+} (5 mol%)-doped CaF_2 nanocrystals at 394 nm. Very sharp emission peaks indicate the nanocrystals are highly crystalline. The energy transfer mechanism of red emission from the Eu^{3+} emitter ion by excitation at 394 nm is shown in Fig. 5(B).

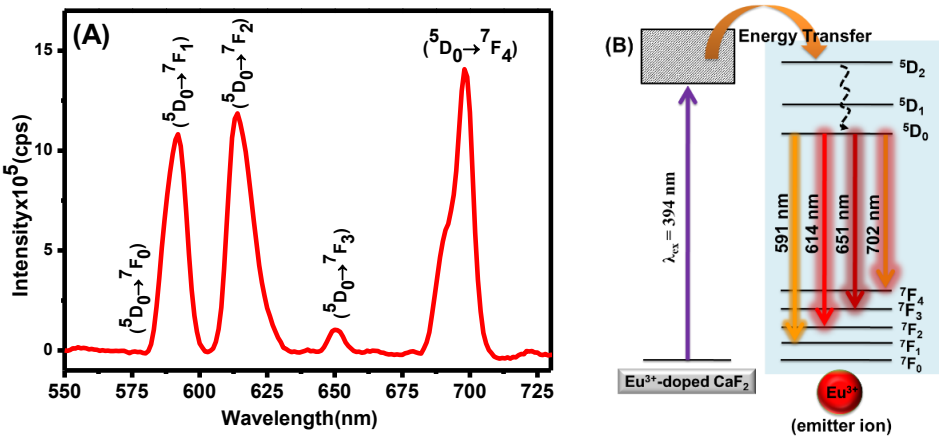

Fig. 5 (A) Photoluminescence emission spectra of Eu^{3+} (5 mol%)-doped CaF_2 nanocrystals in water (λ_{ex} = 394 nm), and (B) energy transfer mechanism for emission from the Eu^{3+} emitter ion.

To check the feasibility of doping another lanthanide ion into the CaF_2 nanocrystals, the study was extended to the Dy^{3+} (2 mol%)-doped CaF_2 nanocrystals. Fig. 6(A) represents the emission spectrum of Dy^{3+} (2 mol%)-doped CaF_2 nanocrystals, in which the blue emission peak at 478 nm is assigned to $^4F_{9/2}\rightarrow{}^6H_{15/2}$ transition while the one close to 580 nm is ascribed to the $^4F_{9/2}\rightarrow{}^6H_{13/2}$ transition. All emission spectra were collected by exciting the aqueous dispersion of Dy^{3+} (2 mol%)-doped CaF_2 nanocrystals at 350 nm. The energy transfer mechanism of blue and yellow emission from the Dy^{3+} emitter ion by excitation at 350 nm is shown in Fig. 6(B) [23].

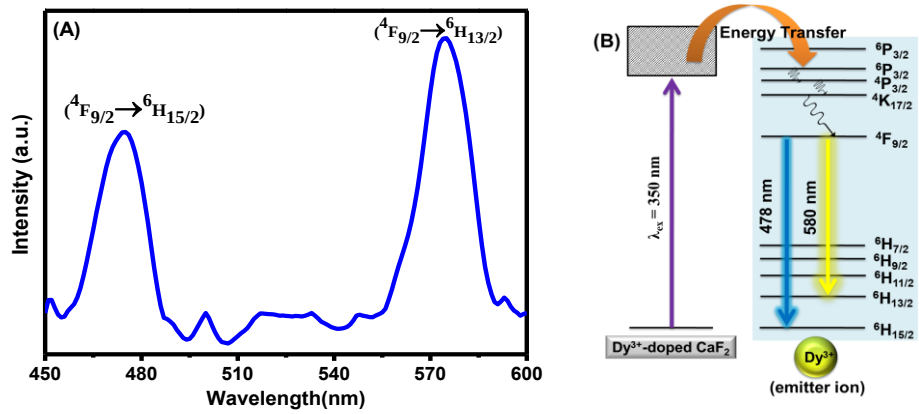

Fig. 6. (A) Photoluminescence emission spectra of Dy^{3+} (2 mol%)-doped CaF_2 nanocrystals in water (λ_{ex} = 350 nm), and (B) energy transfer mechanism for emission from the Dy^{3+} emitter ion.

The photoluminescence lifetimes were calculated using the equation: $I=I_0\exp(t/\tau)$, where I and I_0 are the photoluminescence intensities at the time t and 0, and τ is the photoluminescence lifetime. The measured lifetime value is 1.39 ms for Eu^{3+} (5 mol%)-

doped CaF_2 nanocrystals. The observed trend in the lifetime is supported by the quantum yield measurements as well. The calculated quantum yield values are 12.4 % for Eu^{3+} (5 mol%)-doped CaF_2 nanocrystals. The quantum yield measurements were performed using quinine sulfate as a standard reference. Similarly, the observed lifetime for the 580 nm emission peak is 0.67 ms for Dy^{3+} (2 mol%)-doped CaF_2 nanocrystals. In the same way, the quantum yields of Dy^{3+} (2 mol%)-doped CaF_2 nanocrystals are found to be 4.4 %. This is again measured using quinine sulfate as a reference standard. Longer photoluminescence lifetime and higher quantum yield in both Eu^{3+} (5 mol%)-doped and Dy^{3+} (2 mol%)-doped CaF_2 nanocrystals suggests that CaF_2 is a superior host matrix for lanthanide ions.

4. Conclusion

In summary, the PAA-coated Ln^{3+}-doped (Ln= Eu and Dy) alkaline earth metal fluoride CaF_2 nanocrystals have been made *via* a one-pot hydrothermal method. From FESEM images, the average particle size of the PAA-capped CaF_2 nanocrystals is observed at ~25 nm. Size for Eu^{3+} (5 mol%)-doped CaF_2 nanocrystals, and Dy^{3+} (2 mol%)-doped CaF_2 nanocrystals are found ~23 nm and ~21 nm, respectively. The PAA coating enhances the water dispersibility of the nanocrystals in addition to stabilizing them. Very strong red photoluminescence emission from Eu^{3+} (5 mol%)-doped CaF_2 nanocrystals, along with a longer photoluminescence lifetime (1.39 ms) and quantum yield (12.4 %) suggest that CaF_2 exhibits good optical properties. Moreover, the Dy^{3+} (2 mol%)-doped CaF_2 nanocrystals exhibit strong blue and yellow emissions with a longer photoluminescence lifetime (0.67 ms) and quantum yield (4.4 %). The high dispersibility of the nanocrystals in water, together with intense optical properties, predict that these nanocrystals are well suited for many biological applications and may be used in many fields of optoelectronic devices.

Acknowledgments

The author thanks Ananda Mohan College, Kolkata, for the funding. The author also thanks V. Mahalingam and IISER-Kolkata for providing all instrumental facilities.

References

1. A. Kitai, Luminescent Materials and Its Applications (John Wiley & Sons, 2008).
2. H. Jin, M. Yang, and R. Gui, Nanoscale **15**, 859 (2023). https://doi.org/10.1039/D2NR05721B
3. M. Bungla, S. Chowdhari, M. Shanu, P. Pragya, V. Perumal et al., Phys. Chem. Chem. Phys. **25**, 6131 (2023). https://doi.org/10.1039/D2CP03982F
4. R. Singhaal, L. Tashi, Z. Nisa, N. A. Ashashi, C. Sen et al., RSC Adv. **11**, 19333 (2021). https://doi.org/10.1039/D1RA02910J
5. J. Xu, A. Gulzar, D. Yang, S. Gai, F. He, and P. Yang, Nanoscale **11**, 17535 (2019). https://doi.org/10.1039/C9NR06450H
6. S. Sarkar, M. Chatti, and V. Mahalingam, Chem. Eur. J. **20**, 3311 (2014). https://doi.org/10.1002/chem.201304697

7. S. Sarkar, C. Hazra, and V. Mahalingam, Chem. Eur. J. **18**, 7050 (2012). https://doi.org/10.1002/chem.201103157
8. S. Sarkar, B. Meesaragandla, C. Hazra, and V. Mahalingam, Adv. Mater. **25**, 856 (2013). https://doi.org/10.1002/adma.201203641
9. C. A. Rao, K. Shakampally, and K. V. R. Murthy, J. Sci. Res. **13**, 891 (2021). http://dx.doi.org/10.3329/jsr.v13i3.53287
10. S. K. Basiruddin, J. Sci. Res. **16**, 331 (2024). http://dx.doi.org/10.3329/jsr.v16i1.68491
11. A. Satheesh, D. Adinarayana, M. V. V. Ramanjaneyulu, H. Usha, A. Kumar, and K. N. Jogayya, J. Sci. Res. **16**, 311 (2024). http://dx.doi.org/10.3329/jsr.v16i1.67363
12. V. Sudarsan, F. C. J. M. van Veggel, R. A. Herring, and M. Raudsepp, J. Mater., Chem. **15**, 1332 (2005). https://doi.org/10.1039/B413436B
13. V. Mahalingam, F. Vetrone, R. Naccache, A. Speghini, and J. A. Capobianco, Adv. Mater. **21**, 4025 (2009). https://doi.org/10.1002/adma.200901174
14. S. Sarkar, C. Hazra, and V. Mahalingam, Dalton Trans. **42**, 63 (2013). https://doi.org/10.1039/C2DT31915B
15. S. Sarkar, A. Dash, and V. Mahalingam, Chem. Asian J. **9**, 447 (2014). https://doi.org/10.1002/asia.201301281
16. G. Wang, Q. Peng, and Y. Li, J. Am. Chem. Soc. **131**, 14200, (2009). https://doi.org/10.1021/ja906732y
17. D. Chen, Y. Yu, F. Huang, P. Huang, A. Yang, and Y. Wang, J. Am. Chem. Soc. **132**, 9976 (2010). https://doi.org/10.1021/ja1036429
18. X. Zhang, Z. Quan, J. Yang, P. Yang, H. Lian, and J. Lin, Nanotechnol. **19**, ID 075603 (2008). https://doi.org/10.1088/0957-4484/19/7/075603
19. Z. Yang, G. Wang, Y. Guo, F. Kang, Y. Huang, and D. Bo, Mater. Res. Bull. **47**, 3965 (2012). https://doi.org/10.1016/j.materresbull.2012.08.037
20. E. H. H. Hasabeldaim, H. C. Swart, and R. E. Kroon, RSC Adv. **13**, 5353 (2023). https://doi.org/10.1039/D2RA07897J
21. S. Sarkar, C. Hazra, M. Chatti, V. Sudarsan, and V. Mahalingam, RSC Adv. **2**, 8269 (2012). https://doi.org/10.1039/C2RA21113K
22. L. Wang, Y. Zhang, and Y. Zhu, Nano Res. **3**, 317 (2010). https://doi.org/10.1007/s12274-010-1035-z
23. W. Lü, H. Zhou, G. Chen, J. Li, Z. Zhu , Z. You, C. Tu et al., J. Phys. Chem. C **113**, 3844 (2009). https://doi.org/10.1021/jp8082369